ADSORPTION OF HEAVY METALS FROM WASTEWATER USING MODIFIED RICE HUSK: ISOTHERM, KINETIC, AND MODELING ANALYSIS

N. Das[1], S. Barua[1] and M.S. Islam[1*]

[1]Department of Soil Science, University of Chittagong, Chattogram-4331.

**Corresponding author: msislam@cu.ac.bd*

Abstract

Heavy metal contamination of wastewater presents significant environmental and public health hazards, especially from cationic nickel (Ni^{2+}) and anionic chromium (Cr^{6+}), which exhibit high mobility and toxicity. The present study assessed chemically modified rice husk (MRH) through sequential treatment with citric acid and NaOH, as an adsorbent for the extraction of Ni^{2+} and Cr^{6+} rom aqueous solutions. MRH enhanced their surface area, alkalinity, silica exposure, and reactive functional groups, significantly than the untreated rice husk (RH). MRH adsorbed greater Ni^{2+} and Cr^{6+} than that obtained with RH in both single- and binary-metal systems. Langmuir isotherms significantly fit ($R^2 > 0.98$, $p < 0.05$) the adsorption, signifying monolayer chemisorption, with maximal adsorption capacities of 52.32 mg g^{-1} for Ni^{2+} and 42.35 mg g^{-1} for Cr^{6+}. MRH exhibited greater removal efficiency than that of RH across four adsorption-desorption cycles, indicating remarkable regeneration potential and structural integrity. Comparative analysis with alternative agro-based adsorbents (wheat straw biochar, lemon peel, almond shell activated carbon, and maize straw biochar) demonstrated that MRH ranks among the most efficient materials for Ni^{2+} and shows competitive adsorption for Cr^{6+}. The results proved MRH as a viable and sustainable adsorbent for dual-metal wastewater treatment, providing an effective and environmentally benign option for industrial use.

Keywords: Adsorption Isotherm, Agro-waste adsorbents, Chromium, Kinetic modeling, Nickel, Wastewater treatment

1. Introduction

Heavy metal contamination represents a critical and persistent threat to environmental quality and human health. Nickel (Ni^{2+}) and hexavalent chromium (Cr^{6+}), commonly found as CrO_2^{2-} and $Cr_2O_7^{2-}$, are highly mobile, poisonous, and persistent (Li et al. 2025; Kayranli et al. 2022). Although Cr^{6+} can be reduced to the less dangerous and mobile Cr^{3+} species, it remains a priority pollutant due to its high solubility and bioavailability (Li et al. 2025). Efficient strategies are needed to remove cationic Ni^{2+} and anionic Cr^{6+} using agro-waste adsorbents, which is currently understudied (Dean et al. 2019). Adsorption is widely used in wastewater

treatment because it is simple, cost-efficient, and effective (Liu et al. 2020). Nonetheless, identifying environmentally friendly and cost-effective adsorbents remains a difficulty. Although many synthetic adsorbents show impressive performance, they are expensive, environmental hazardous, and non-renewable (Liang et al. 2022). Agricultural and industrial byproducts appeared a feasible alternative by transforming waste materials into cost-effective wastewater treatment resources (Dinh et al. 2021). Agricultural byproducts such as rice husk (RH) are often used to remove pollutants from water (Islam et al. 2022). RH accounts for about one-fifth of global rice output (545 million tons), with Bangladesh producing more than 9 million tons annually (Islam & Ahiduzzaman, 2013). RH contains cellulose, hemicellulose, lignin, and silica, makes a suitable precursor for porous adsorbents (Liu et al. 2020). However, raw RH has limited adsorption capacity, necessitating chemical treatment to improve surface functionality and performance (Liu et al. 2020; Kurniasih et al. 2025; Zhou et al. 2025). Alkali activation and functional group insertion to RH using NaOH and citric acid (CA) greatly improved its adsorption efficiency (Kurniasih et al. 2025). Treated materials improved processes including electrostatic attraction, ion exchange, hydrogen bonding, π-π interactions, and chemisorption (Kurniasih et al. 2025; Zhou et al. 2025). While MRH has potential, most research focused on single-metal systems or provides generalized performance data without explaining the fundamental principles (Dinh et al. 2021; Zhou et al. 2025; Kurniasih et al. 2025). The competitive behavior of cationic and anionic metals on RH surfaces treated with NaOH or CA is so confusing that the impact of NaOH and CA loading on surface reactivity and stability under diverse chemical conditions is little understood. Some studies investigated the reusability of RH and MRH during four adsorption-desorption cycles to assess long-term sustainability (Liu et al. 2020; Zhou et al. 2025; Kurniasih et al. 2025). They reported that the chemically modifying RH (MRH) improved its structural and surface properties, leading to better adsorption of Ni^{2+} and Cr^{6+} than plain RH. We hypothesized that MRH would be stable and reusable across multiple adsorption-desorption cycles, with effective performance in both single and binary metal systems. The reported adsorption capabilities for Ni^{2+} and Cr^{6+} utilizing agro-waste-derived adsorbents exhibit significant variability based on the precursor and modification method employed. Consequently, comparing MRH performance with other adsorbents offers valuable background for assessing its practical viability as an economical dual-metal sorbent. The present study aims to (i) modify and characterize MRH using CA and NaOH; (ii) assess the adsorption capacities of MRH for Ni^{2+} and Cr^{6+} in both single and binary metal systems; (iii) explore adsorption mechanisms through isotherm and kinetic models alongside surface analyses (BET, zeta potential); and (iv) evaluate reusability and stability across multiple adsorption-desorption cycles.

2. Materials and Methods

2.1 Materials and chemicals

The rice husk (RH) was acquired locally and utilized analytical grade chemicals for the experiment. The chemicals include nickel nitrate ($Ni(NO_3)_2$, 99%), potassium dichromate

($K_2Cr_2O_7$, 99.5%), citric acid (CA, 99%), and sodium hydroxide (NaOH, 97%), sourced from Merck (Germany). The additional chemicals utilized in this experiment were of analytical quality (Merck, Germany). Distilled water was utilized for solution formulation and rinsing.

2.2 Modification of adsorbent material

2.2.1 Processing of rice husk

The collected RH was washed three times with distilled water (solid-liquid ratio 1:10), agitated for 60 minutes at 200 rpm, centrifuged, dried at 60°C, and sieved to <250 µm before use.

2.2.2 Preparation of modified rice husk

The RH was coupled with 0.5 M CA (1:12 w/v) for 30 minutes at ambient temperature to generate modified RH (MRH), which was then heated to 120 °C for 90 minutes, washed, and filtered. The material was treated with 0.1 M NaOH for 60 minutes, rinsed, dried at 60 °C, and crushed to a particle size of <250 µm before analysis (Kazembeigi et al., 2014).

2.3 Adsorbent characterization

The moisture content of RH and MRH was determined using Black's (1965) approach, and pH was measured in distilled water at a 1:20 (w/v) ratio using a pH meter (Hanna HI3M) (Jackson, 1958). The specific surface area was calculated using the Brunauer-Emmett-Teller (BET) method with nitrogen adsorption at 77 K (Dogan et al., 2006). The cellulose, hemicellulose, and lignin contents were determined using standard biochemical procedures, whereas the ash content was determined by incinerating samples at 750 °C for 1 hour in an open crucible (Salam et al., 2019).

The zeta potential was assessed in accordance with Jiang et al. (2012). Adsorbents (0.2 g; RH and MRH) were suspended in 250 mL of 0.01 M $NaNO_3$. The pH was adjusted to 2 with 0.1M HCl and 10 with 0.1 M NaOH. Suspensions were ultrasonically agitated for an hour before being equilibrated at room temperature for 24 hours. Measurements were taken in triplicate using a zeta analyzer (Nano Partica SZ-100V2 analyzer, HORIBA) at 50-200 mV and 10-50 readings per sample.

2.4 General batch adsorption conditions

Batch experiments were carried out at 25°C with 1 g L^{-1} of adsorbent in 100 mL of metal solution (100 mg L^{-1} of Ni^{2+}, Cr^{6+}, or a 1:1 combination of Ni^{2+} and Cr^{6+}) at pH 5.5. Suspensions were agitated (120 rpm, 360 min) until equilibrium, filtered (0.22 µm), and evaluated using an atomic absorption spectrophotometer (AAS) 240 AA (Agilent Technologies, Australia).

2.5 Adsorption studies

2.5.1 Impact of solution pH on metal adsorption

The adsorption of Ni^{2+} and Cr^{6+} at pH ranges of 2 to 10 was measured using 0.1 g of adsorbent per 100 mL of solution (100 mg L^{-1} of Ni^{2+} or Cr^{6+}). The adsorption capacity (q, mg g^{-1}) and removal efficacy (R, %) of metal were determined using the following equations (Zhang et al. 2020):

Adsorption capacity: $$q = \frac{(C_o - C_1)v}{m} \quad \text{---------- (1)}$$

Removal efficiency: $$R = \frac{(C_o - C_1)}{C_o} X\ 100 \quad \text{---------- (2)}$$

In this context, q represents the adsorption quantity, Co (mg L^{-1}) is the starting analyte concentration, C (mg L^{-1}) is the final analyte concentration, V (L) is the analyte solution volume, and m (g) is the adsorbent mass.

2.5.2 Influence of coexisting metals on metal adsorption

The influence of Ni^{2+} or Cr^{6+} concentration on their adsorption in both single and competing metal systems is delineated below (Zeng et al. 2024):

(i) Single-metal adsorption: Influence of starting concentrations of Ni^{2+} or Cr^{6+} ranging from 10 to 200 mg L^{-1} on distinct adsorption behavior.

(ii) Adsorption of Ni^{2+} in the presence of Cr^{6+}: The initial concentration of Ni^{2+} was maintained at 100 mg L^{-1}, while the concentration of Cr^{6+} was adjusted to establish initial Ni^{2+} to Cr^{6+} concentration ratios of 1:0, 1:1, 1:2, 1:4, and 1:8 to examine the effect of Cr^{6+} on the adsorption of Ni^{2+}.

(iii) Adsorption of Cr^{6+} in the presence of Ni^{2+}: The starting concentration of Cr^{6+} was 100 mg L^{-1}, while the concentration of Ni^{2+} was incrementally elevated to establish Ni^{2+}: Cr^{6+} ratios of 0:1, 1:1, 2:1, 4:1, and 8:1 to examine the influence of Ni^{2+} on Cr^{6+} adsorption.

Adsorption equilibrium data for individual metals were modeled utilizing the nonlinear Langmuir (Eq. 3) and Freundlich (Eq. 4) isotherms (Foo & Hameed, 2010):

Langmuir isotherm: $$q_e = \frac{q_m k_L C_e}{1 + k_L C_e} \quad \text{---------- (3)}$$

Freundlich isotherm: $$q_e = k_F C_e^{\,1/n} \quad \text{---------- (4)}$$

Ce (mg L^{-1}) represents the equilibrium concentration of Ni^{2+} and Cr^{6+}, qm (mg g^{-1}) represents the theoretical maximum adsorption capacity, K_L (L mg^{-1}) reflects the Langmuir adsorption constant associated with binding affinity, KF ((mg g^{-1}) (L $mg^{-1})^{1}/^{n}$) denotes the Freundlich constant pertaining to adsorption capacity, and 1/n represents the heterogeneity factor, which indicates surface heterogeneity and adsorption intensity.

Nonlinear regression was used to determine model parameters, as well as their related uncertainties and 95% confidence intervals. Raw fitting charts, which compare experimental and model-predicted adsorption capabilities, as well as residual analysis, were used to assess model adequacy. The residual plots were used to ensure that errors were random and uniformly distributed, as well as to assess the adsorption models' goodness of fit.

2.6 Kinetic studies

Kinetic adsorption experiments for Ni^{2+} and Cr^{6+} were conducted throughout durations of 0 to 360 minutes under consistent batch conditions. The 360-minute duration was used as the endpoint to guarantee adsorption equilibrium, as documented by Lyu et al. (2022). The data were examined utilizing the non-linear variants of the pseudo-first-order and pseudo-second-order models (Ho & McKay, 1999):

Pseudo-first order: $qt = qe\,(1 - e^{-k_1 t})$ ---------- (5)

Pseudo-second order: $$qt = \frac{k_2 qe^{2} t}{1 + k_2 qe^{2} t}$$ ---------- (6)

In this context, qt (mg g^{-1}) denotes the anticipated adsorption capacity at time t; qe (mg g^{-1}) indicates the equilibrium adsorption capacity; k_1 (min-1) and k_2 (g (mg min)$^{-1}$) represent the pseudo-first order and pseudo-second order rate constants, respectively; and t (min) denotes the duration of contact. The model parameters were calculated using non-linear regression and 95% confidence intervals, as described in Section 2.5.2. The model's suitability was assessed by comparing experimental and model-predicted qe performance, as well as performing a residual analysis.

2.7 Desorption and regeneration studies

For regeneration testing, 0.1 g of each adsorbent was combined with 100 mL of Ni^{2+} or Cr^{6+} solutions at pH 5.5, with initial Ni^{2+} and Cr^{6+} concentrations of 100 mg L^{-1} (Deng *et al.* 2013). The solutions were stirred at room temperature for 300 minutes before being reactivated by immersing in 320 mL of elution solution (0.5 M HCl for Ni^{2+} and 0.5 M NaOH for Cr^{6+}) for 4 hours (Huang *et al.* 2018) and centrifuged at 3000 rpm for 10 minutes. The regenerated

adsorbents were then washed with ultrapure water and prepared for future adsorption cycles. The adsorption-desorption cycle was repeated four times.

2.8 Quality assurance and statistical analysis

Data from all experiments were analyzed in triplicate and presented as mean ± SD. To produce parameter errors, nonlinear regression fitting was used using experimental uncertainties. Model performance and appropriateness were assessed using the coefficient of determination. Treatment differences were analyzed using one-way ANOVA and Tukey's post hoc test ($p < 0.05$) in SPSS version 22. All curve fits and regressions were done with Origin Pro 2021.

3. Results and discussion

3.1 Adsorbent characterization

The alteration significantly enhanced the characteristics of the RH (Table 1). The pH rose from 6.50 to 7.70, rendering the material's surface more alkaline, which enhanced its capacity for binding metal ions. The surface area increased significantly from 20.75 to 92.65 $m^2\ g^{-1}$, signifying the formation of new pores and enhanced adsorption sites (Liu *et al.* 2020).

Table 1. Physical and chemical analysis of unmodified and modified rice husk (mean ± SD)

Parameters	Rice husk (RH)	Modified rice husk (MRH)
pH	6.50±0.76	7.70±0.55
Moisture content (%)	6.60±0.55	6.20±0.47
Surface area ($m^2\ g^{-1}$)	20.75±1.12	92.65±1.85
Ash Content (%)	23.65±1.23	15.52±0.96
Cellulose (%)	34.53±1.54	54.35±1.14
Hemicellulose (%)	20.72±1.02	16.83±1.00
Lignin (%)	19.62±1.11	12.65±0.86
Silica (SiO_2)	17.85±1.05	97.55±1.94

Alterations in composition further illustrate the impact of the treatment. The decrease in ash coupled with the significant rise in silica indicates that contaminants were eliminated, hence revealing the silica-rich structure more prominently. Simultaneously, cellulose grew while hemicellulose and lignin decreased (Table 1), indicating that less-ordered components

were partially eliminated, resulting in a greater availability of reactive hydroxyl groups for metal absorption (Liu *et al.* 2020). The enhanced surface area, elevated alkalinity, and greater abundance of reactive groups elucidate why the MRH is more effective for metal adsorption compared to the unprocessed material. The pHpzc values for RH and MRH were 5.0 and 5.5, respectively (Fig. 1). The surface charge of the adsorbents determines the adsorption behavior of Ni^{2+}, a cationic metal, and Cr^{6+}, an anionic metal; hence, the solution pH dictates these behaviors in relation to the pHpzc (Liu *et al.* 2020; Msimango *et al.* 2025). At pH values below pHpzc, the adsorbent surfaces acquire a positive charge, causing electrostatic repulsion of the cationic Ni^{2+} and attraction of the anionic Cr^{6+}. Conversely, above pHpzc, the surface charge becomes negative, therefore improving Ni^{2+} adsorption by electrostatic attraction and lowering Cr^{6+} adsorption. These zeta potentials closely match with the pH-dependent adsorption behavior (Liu *et al.* 2020; Msimango *et al.* 2025).

3.2 Adsorption study

3.2.1 Impact of initial pH on metal adsorption

Metal adsorption on RH and MRH depends on solution pH, with MRH adsorbing more than RH (Fig. 2). Ni^{2+} adsorption capacity of RH and MRH increased with pH, peaking at pH 8. Alkaline conditions increase adsorption efficiency because negatively charged surface functional groups, notably deprotonated-COOH groups, interact electrostatically with positively charged Ni^{2+} molecules (Liu *et al.* 2020). However, Cr^{6+} adsorption is enhanced in very acidic conditions, peaking at pH 3 (Fig. 2). The -COOH groups of RH and MRH remained protonated at low pH, creating a positively charged adsorbent surface that attracts negatively charged Cr^{6+} molecules. Surface modification boosts functional group availability and optimizes pH-dependent adsorption behavior, enhancing Ni^{2+} and Cr^{6+} removal efficiency (Liu *et al.,* 2020).

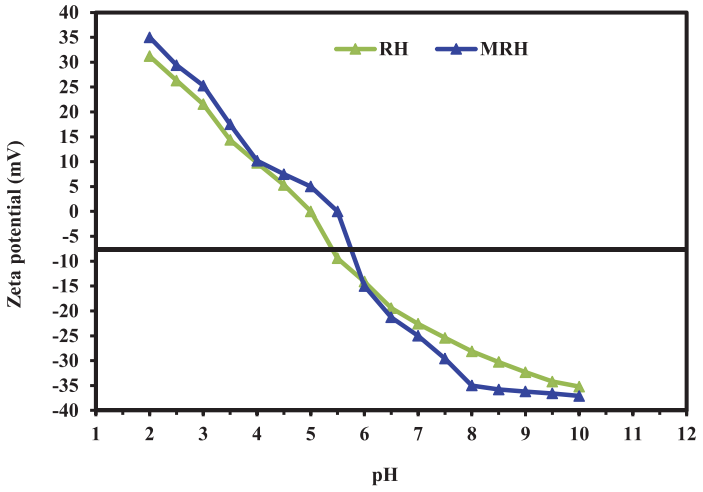

Fig. 1 Zeta potential of raw and modified RH to explore changes in surface charge that influence heavy-metal adsorption

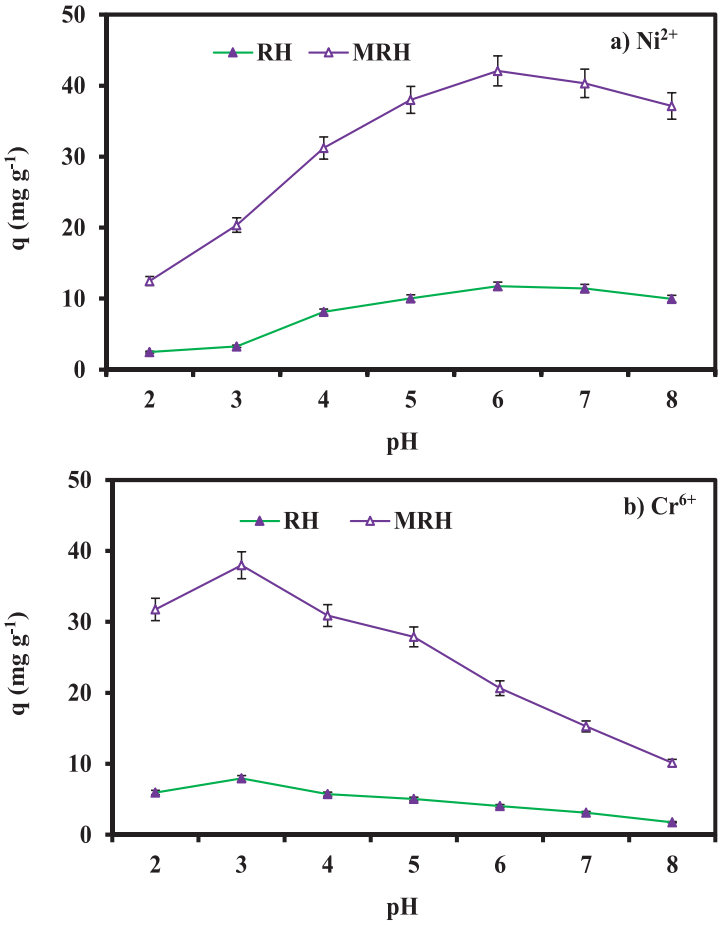

Fig. 2 Effects of initial solution pH on the adsorption of Ni^{2+} (a) and Cr^{6+} (b) by RH and MRH, to evaluate the role of solution pH on metal adsorption behavior (mean ± SD (n = 3)

3.2.2 Impact of coexisting metals on metal adsorption

Adjacent ions had a considerable effect on metal adsorption, suggesting both individual and competitive interactions (Figs. 3-4). Ni^{2+} and Cr^{6+} adsorption increased from 10 to 200 mg L^{-1}, with MRH exhibiting high adsorption capabilities (Ni^{2+}: 46.00 mg g^{-1}, 23.00% removal; Cr^{6+}: 37.23 mg g^{-1}, 18.62% removal) compared to RH (Ni^{2+}: 9.01 mg g^{-1}, 4.51% removal; Cr^{6+}: 8.40 mg g^{-1}, 4.20%). The differences reflect the increased surface area, functional groups, and electrostatic properties formed during the modification process, which improves metal binding (Liu et al. 2020). Fig. 3-4 and Table 2 show the Langmuir and Freundlich isotherms, as well as the raw fitting and residual analyses. The Langmuir model provided the best match (R^2 > 0.99 and randomly distributed residuals), indicating a probable monolayer chemisorption. The predicted qm values for MRH were the highest (Ni^{2+}: 52.32 mg g^{-1}; Cr^{6+}: 42.36 mg g^{-1}), but

the Freundlich fits were not quite right (Table 2). These findings suggest that adsorption might occur on homogeneous active sites with strong binding energies (monolayer adsorption), which corresponds to the surface uniformity generated by modification (Kayranli et al. 2022).

Table 2. Langmuir and Freundlich isotherm parameters for Ni^{2+} and Cr^{6+} adsorption onto RH and MRH in single-metal systems, highlighting their contribution to adsorption efficiency (mean ± SD, n = 3)

Pollutants	Model	Parameters	Adsorbents	
			RH	MRH
Ni^{2+}	Langmuir	*qm (mg g^{-1})*	10.65±0.05	52.32±1.78
		K_L (L mg^{-1})	0.02762±0.00	0.038239±0.02
		R^2	0.998±0.03	0.993±0.03
		p value	2.96x10^{-7}±0.00	3.2x10^{-11}±0.00
	Freundlich	*K_F ((mg g^{-1}) (L mg^{-1})$^{1/n}$)*	1.25286768±0.04	6.77530901±0.07
		1/n	0.387958±0.02	0.391556±0.01
		R^2	0.960±0.02	0.976±0.02
		p value	3.23x10^{-4}±0.03	9.1x10^{-5}±0.03
Cr^{6+}	Langmuir	*qm (mg g^{-1})*	10.56±0.04	42.36±1.11
		K_L (L mg^{-1})	0.021886±0.00	0.048693±0.00
		R^2	0.993±0.03	0.998±0.02
		p value	4.75x10^{-6}	1.12x10^{-7}
	Freundlich	*K_F ((mg g^{-1}) (L mg^{-1})$^{1/n}$)*	1.253±0.04	6.775309±0.45
		1/n	0.38796±0.02	0.391556±0.01
		R^2	0.960±0.02	0.976±0.02
		p value	3.23x10^{-4}	9.10x10^{-5}

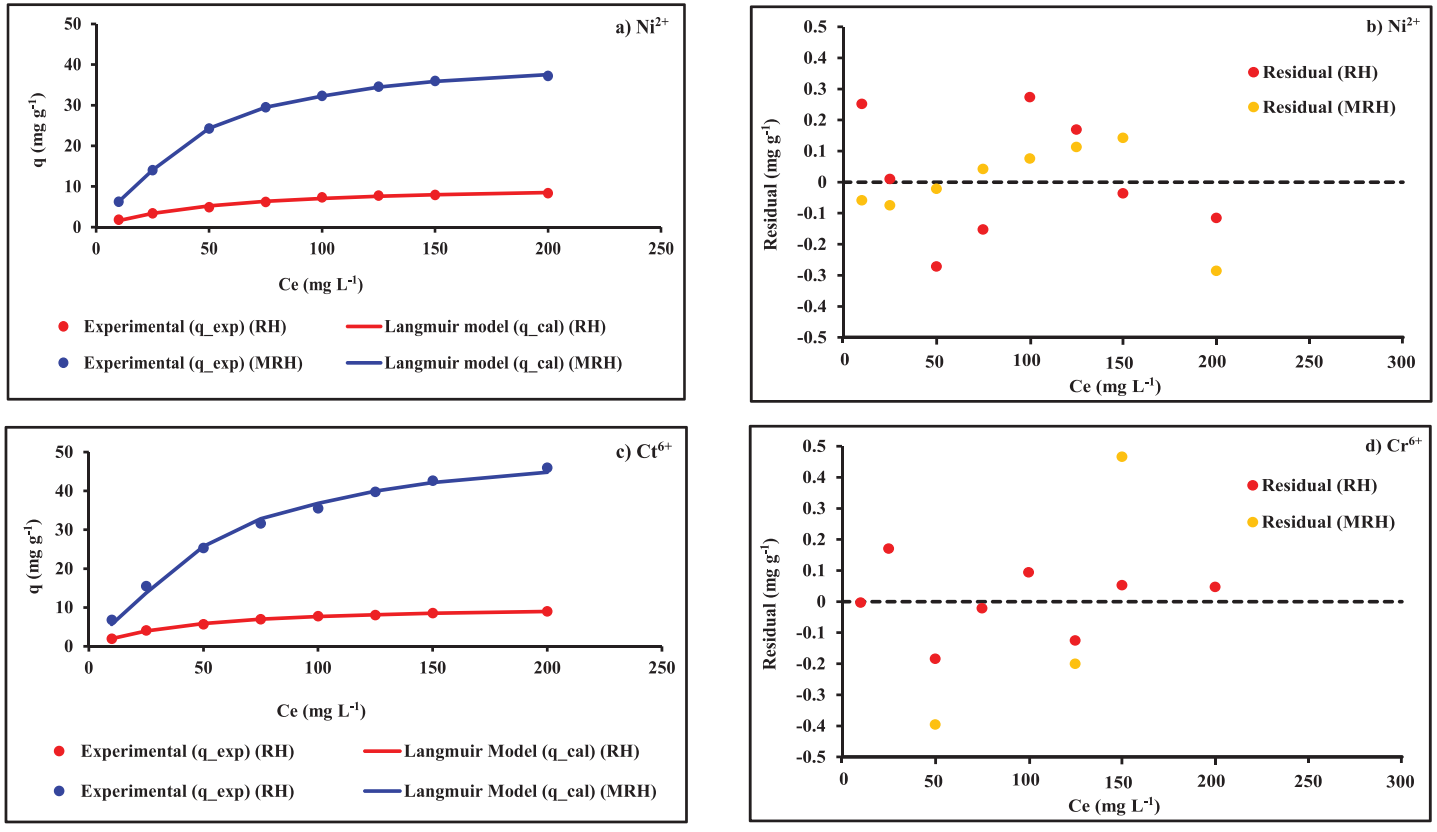

Fig. 3 Effects of initial Ni^{2+} and Cr^{6+} concentrations on experimental and model-predicted adsorption capacities and residuals for Ni^{2+} (a, b) and Cr^{6+} (c, d) using the Langmuir model for RH and MRH, showing adsorption behavior and model fitting accuracy

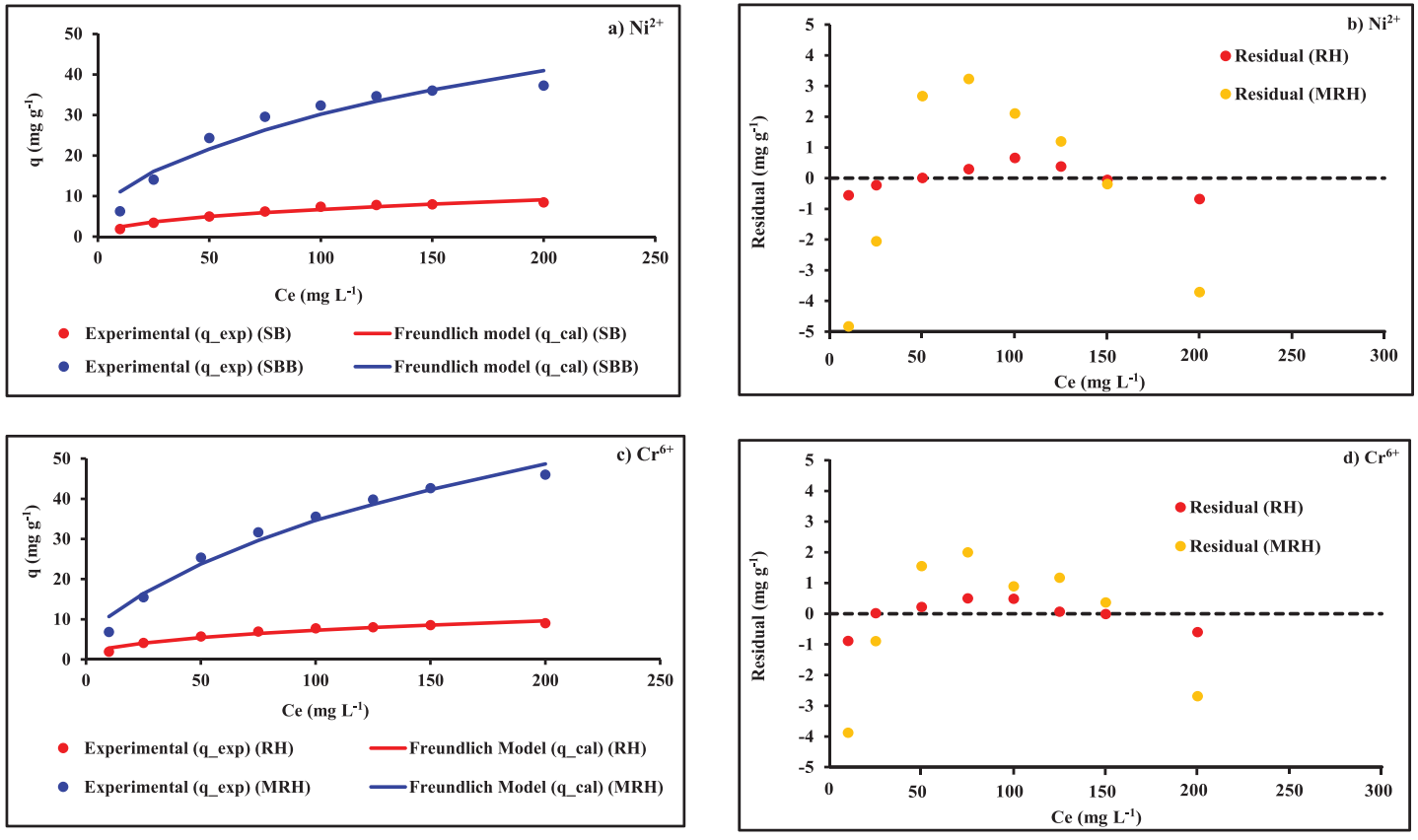

Fig. 4 Effects of initial Ni^{2+} and Cr^{6+} concentrations on experimental and model-predicted adsorption capacities and residuals for Ni^{2+} (a, b) and Cr^{6+} (c, d) using the Freundlich model for RH and MRH, showing adsorption behavior and model fitting accuracy.

Within the realm of agro-waste-derived adsorbents, the Ni^{2+} Langmuir capacity of MRH (52.32 mg g^{-1}) is comparable to numerous documented biochars and unmodified wastes, such as wheat straw biochar, rice husk biochar, lemon peel, almond shell activated carbon, and sugarcane bagasse (Kayranli *et al.* 2022; Msimango *et al.* 2025). Some chemically treated materials exhibit enhanced adsorption capabilities, such as modified rice husk (86.00 mg g^{-1}) and modified sugarcane bagasse (125.70 mg g^{-1}) (Msimango *et al.* 2025). The CA/NaOH alteration significantly improves Ni^{2+} binding relative to unmodified RH. For Cr^{6+}, MRH demonstrates a moderate Langmuir adsorption capacity of approximately 42.35 mg g^{-1}, which is comparable to certain low-cost biochars, such as lemon-peel biochar (Ahmadian *et al.,* 2022), yet inferior to specialized engineered adsorbents, including nitrogen-doped biochars and maize straw biochar (Li *et al.,* 2025). Nonetheless, MRH surpasses most untreated or minimally modified agricultural by-products (Liang *et al.* 2022), underscoring its viability as an efficient Cr^{6+} adsorbent where simplicity and cost-effectiveness are paramount.

Adsorption in the mixed-metal system was not significantly reduced by competitive interactions. Ni^{2+} absorption increased from 34.24 to 68.56 mg g^{-1} (34.24 to 68.56%) as Cr^{6+} concentration increased to 800 mg L^{-1}, indicating a synergistic effect (Table 3). Cr^{6+} adsorption increased with higher Ni^{2+} concentrations (32.12 to 62.03 mg g^{-1}, 32.12 to 62.03%), but not as significantly as Ni^{2+} (Table 4). These patterns indicate that coexisting metals interact in both competitive and cooperative ways, either by altering surface charge or disclosing more sites (Kayranli et al., 2022; Liu et al., 2020). The higher adsorption of Ni^{2+} might be due to its greater affinity and enhanced sensitivity to surface changes. The findings show that MRH outperforms RH in both single- and dual-metal systems and that competitive and synergistic interactions might influence adsorption behavior in mixed-metal situations (Kayranli *et al.,* 2022; Liu *et al.,* 2020).

Table 3. Adsorption efficacy of RH and MRH for Ni^{2+} and Cr^{6+} at 100 mg L-1 Ni^{2+} concentration with increasing Cr^{6+} concentrations, highlighting their distinct contributions to dual metal elimination (mean ± SD, n = 3)

Cr^{5+} (mg L^{-1})	Adsorption capacity, q (mg g^{-1})			
	RH		MRH	
	Ni^{2+}	Cr^{6+}	Ni^{2+}	Cr^{6+}
0	7.38±0.75c	0.00±0.00e	34.24±2.43e	0.00±0.00e
100	8.97±1.02c	6.95±0.76d	40.46±2.17d	31.87±1.75d
200	10.25±1.04b	27.69±1.28c	44.54±2.54c	92.64±2.36c
400	11.48±0.97b	72.81±2.32b	52.75±1.88b	240.53±3.75b
800	14.05±1.15a	116.85±3.58a	68.56±1.57a	398.74±3.87a

Means with different letters in the same column differ significantly at $p < 0.05$ (Turkey's post hoc test)

Table 4. Adsorption efficacy of RH and MRH for Ni^{2+} and Cr^{6+} at 100 mg L-1 Cr^{6+} with increasing Ni^{2+} concentrations, highlighting their distinct contributions to dual metal elimination (mean ± SD, n = 3)

Ni^{2+} ($mg\ L^{-1}$)	Adsorption capacity, q ($mg\ g^{-1}$)			
	RH		MRH	
	Ni^{2+}	Cr^{6+}	Ni^{2+}	Cr^{6+}
0	0.00±0.00e	7.28±0.76c	0.00±0.00e	32.12±1.15d
100	7.08±0.87d	8.28±0.88c	34.23±2.14d	36.02±1.08c
200	17.57±1.12c	8.81±0.58c	138.78±3.54c	38.64±1.10c
400	46.97±1.87b	10.65±1.01b	294.56±3.78b	45.12±1.35b
800	112.68±2.48a	12.37±1.12a	398.74±3.90a	62.03±2.18a

Means with different letters in the same column differ significantly at $p < 0.05$ (Turkey's post hoc test)

3.3 Kinetic studies

The adsorption kinetics of Ni^{2+} and Cr^{6+} on RH and MRH were analyzed to ascertain the duration and potential mechanism of metal removal from the system (Figs. 5-6; Table 5). Both metals exhibited swift initial absorption within the first 60 minutes, followed by a decelerated rate, achieving equilibrium between 180 and 360 minutes. This pattern signifies swift colonization of plentiful surface places at first, succeeded by gradual spread into more inaccessible areas (Liu *et al.,* 2020). The highest equilibrium adsorption capacity and removal were observed for MRH (Ni^{2+}: 37.00 mg g^{-1}, 37.00%; Cr^{6+}: 34.00 mg g^{-1}, 34.00%), succeeded by RH (Ni^{2+}: 7.25 mg g^{-1}, 7.25%; Cr^{6+}: 6.95 mg g^{-1}, 6.95%). The significant increase post-modification indicates improved functional groups and enhanced binding affinity on MRH (Liu *et al.,* 2020). At 60 min, MRH had adsorbed 34.12 mg g^{-1} (34.12%) of Ni^{2+} and 30.88 mg g^{-1} (30.88%) of Cr^{6+}, achieving 93.38% and 90.08% of its equilibrium capacity, respectively (Figs. 5-6).

This indicates that the majority of adsorption transpired swiftly owing to the readily available active sites (Msimango et al. 2025). The pseudo-second-order model demonstrated the most accurate fit for Ni^{2+} (R^2 0.98-0.99) and Cr^{6+} (R^2 0.98); however, the pseudo-first-order models were inadequate (Ni^{2+}: R^2 0.87-0.95; Cr^{6+}: R^2 0.92) (Table 5). This optimal fit indicates that chemisorption might be the primary process, possibly governed by electron transfer and robust surface coordination. Surface complexation and π-π interactions might enhance chemisorption, as demonstrated by random residuals and a strong correlation between

predicted and experimental qe in the pseudo-second order relative to pseudo-first order (Figs. 5-6; Table 5). These findings suggest that altered surfaces promote enhanced bonding interactions, might elucidating the accelerated kinetics and superior capacity of MRH in comparison to RH (Msimango *et al.* 2025; Liu *et al.* 2020).

3.4 Desorption and regeneration study

The effectiveness of regeneration is a crucial factor for evaluating the long-term sustainability of adsorbents in wastewater treatment. MRH exhibited exceptional stability and reusability during four adsorption-desorption cycles, with negligible declines in metal removal effectiveness (Ni^{2+}: 90.05% to 92.87%; Cr^{6+}: 80.44% to 85.08%) (Fig. 6). This minor decline indicates that the most active sites may persist, exhibiting strong structural integrity and resilient surface chemistry (Msimango *et al.,* 2025; Liu *et al.,* 2020).

Conversely, RH demonstrated considerable efficiency declines, with fourth-cycle adsorption decreasing to 70.62% for Ni^{2+} and falling below 70% (64.55%) for Cr^{6+}. The improved regenerative characteristics of MRH are attributed to its stable Fe–O and hydroxyl groups, which may facilitate reversible chemisorption and sustain electrostatic equilibrium with repeated applications (Msimango *et al.,* 2025; Liu *et al.,* 2020). The results, together with the data on adsorption and kinetics, offer a thorough understanding of the adsorption mechanisms and highlight the considerable potential of MRH for effective wastewater treatment.

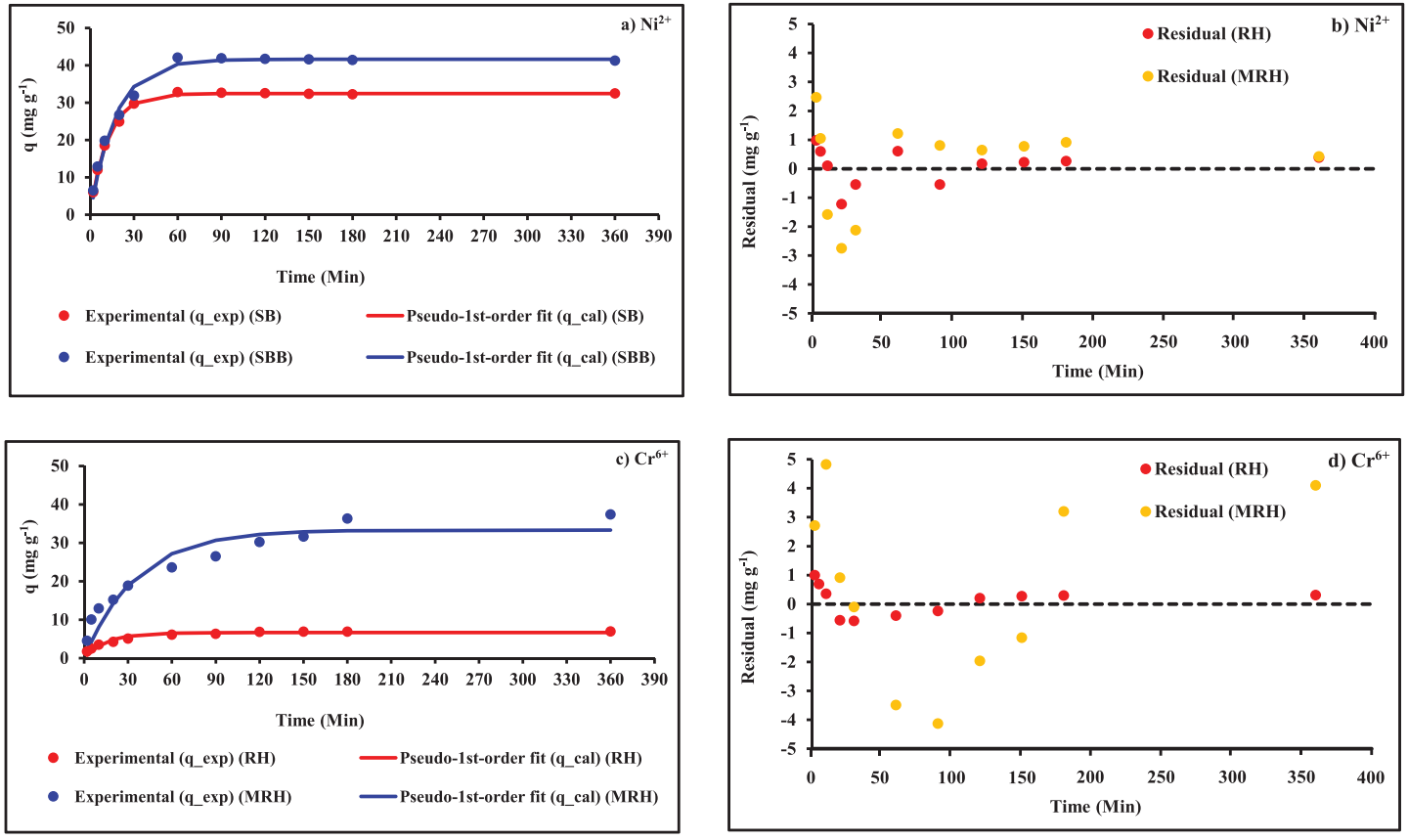

Fig. 5 Effects of contact time on experimental and model-predicted adsorption capacities and residuals for Ni^{2+} (a, b) and Cr^{6+} (c, d) using the pseudo-first-order kinetic model for RH and MRH, showing adsorption behavior and model fitting accuracy

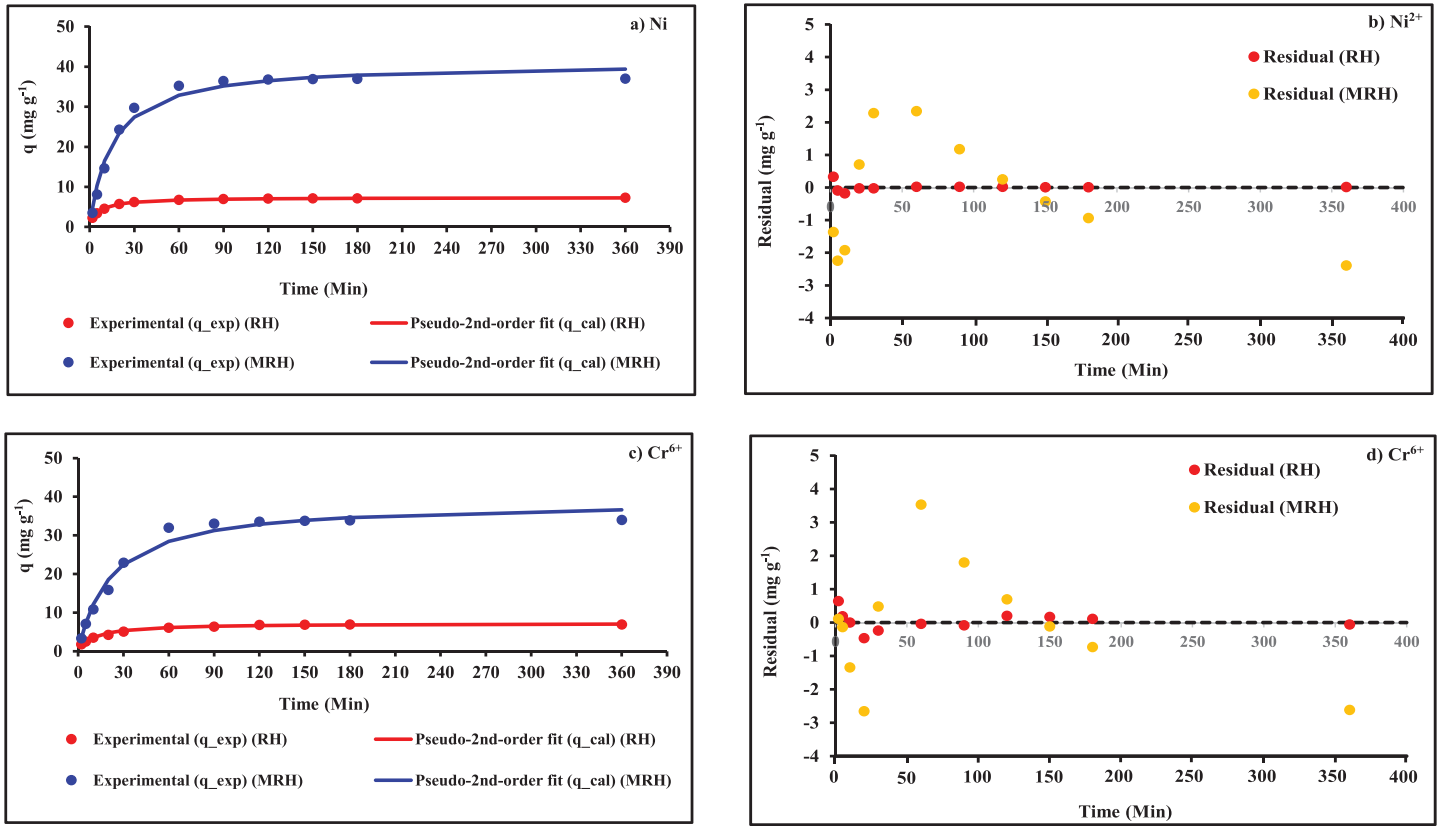

Fig. 6 Effects of contact time on experimental and model-predicted adsorption capacities and residuals for Ni^{2+} (a, b) and Cr^{6+} (c, d) using the pseudo-second-order kinetic model for RH and MRH, showing adsorption behavior and model fitting accuracy

Table 5. Kinetic model parameters (pseudo-first-order and pseudo-second-order) for Ni2+ and Cr6+ adsorption onto RH and MRH in single-metal systems, contributing to adsorption mechanism analysis (mean ± SD, n = 3)

Pollutants	Model	Parameters	Adsorbents	
			RH	MRH
Ni^{2+}	Pseudo-first-order	*qm (mg g^{-1})*	6.87±0.32	32.76±1.21
		k_1 (min^{-1})	0.103966±0.04	0.160276±0.02
		R^2	0.868±0.03	0.953±0.02
	Pseudo-second-order	*qm (mg g^{-1})*	7.34±0.22	41.01±1.32
		K_2 (g mg^{-1} min^{-1})	0.024424±0.00	0.001643±0.00
		R^2	0.995±0.02	0.982±0.01
Cr^{6+}	Pseudo-first-order	*qm (mg g^{-1})*	6.64±0.32	33.52±1.21
		k_1 (min^{-1})	0.065397±0.00	0.03036±0.00
		R^2	0.923±0.02	0.920±0.02
	Pseudo-second-order	*qm (mg g^{-1})*	7.20±0.06	38.84±1.32
		K_2 (g mg^{-1} min^{-1})	0.013395±0.00	0.001178±0.00
		R^2	0.977±0.02	0.978±0.02

Table 6. Regeneration study of RH and MRH for Ni^{2+} and Cr^{6+} adsorption to explore their reusability and long-term adsorption stability (mean ± SD, n = 3)

Cycles	Removal efficiency of Ni^{2+} (%)		Removal efficiency of Cr^{6+} (%)	
	RH	MRH	RH	MRH
Cycle 1	76.23±1.12	92.87±1.85	69.28±1.82	85.08±2.16
Cycle 2	74.29±1.07	92.15±1.77	68.45±1.94	84.12±1.59
Cycle 3	72.88±1.42	91.37±1.90	66.61±1.05	82.12±1.62
Cycle 4	70.62±1.17	90.05±1.45	64.55±1.55	80.44±1.28

4. Conclusions

This study illustrates that citric acid and alkali alteration significantly improved the structural, chemical, and adsorption characteristics of rice husk (RH), converting it into an effective and sustainable adsorbent for the removal of Ni^{2+} and Cr^{6+}. The modified rice husk (MRH) demonstrated a markedly increased surface area, enhanced surface charge characteristics, and a greater abundance of functional groups. Adsorption exhibited significant pH dependence, with MRH attaining optimal Ni^{2+} absorption in mildly alkaline settings and Cr^{6+} uptake in acidic conditions. The equilibrium results were optimally represented by the Langmuir model, signifying probable monolayer chemisorption; however, kinetic analysis validated pseudo-second-order kinetics, implying possible robust surface contacts and electron-sharing mechanisms. MRH exhibited consistent removal effectiveness over several adsorption-desorption cycles, affirming its structural integrity and reusability. The findings proved MRH as a viable, environmentally sustainable material for the treatment of mixed-metal wastewater. Additional research is recommended to test MRH effectiveness in actual industrial effluents, evaluate long-term operational stability, and improve large-scale implementation for effective wastewater treatment systems.

Acknowledgements

The authors wish to express profound gratitude to the University Grants Commission of Bangladesh for the financial support (Grant number: Agricultural Science (Crop science-8)/2022-2023) for this research.

Conflicts of Interest

The authors declare that they have no conflicts of interest for the publication of this paper.

References

Ahmadian, A., Goharrizi, B.A., Shahriari, T. and Ahmadi, S. 2022. Adsorption of chromium (VI) and acid orange 7 on lemon peel biochar: a response surface methodology approach. Inter. Jour. Environ. Sc. and Tech. 20: 2939–2958.

Black, C.A. 1965. Methods of Soil Analysis. Part I, American Society of Agronomy. Madison, Wisconsin.

Dean, A.M.K.E., Hashem, E.Y., Ahmed, M.M., Mohamed, M.A. and Hussain, S.M. 2019. Removal of chromium (VI) from wastewater using citric acid modified sugarcane bagasse. Eur. Chem. Bull. 8: 141.

Deng, J., Zhang, X., Zeng, G., Gong, J., Niu, Q. and Liang, J. 2013. Simultaneous removal of Cd(II) and ionic dyes from aqueous solution using magnetic graphene oxide nanocomposite as an adsorbent. Chem. Eng. J. 226: 189–200.

Dinh, N.T., Vo, L.N.H., Tran, N.T.T., Phan, T.D. and Nguyen, D.B. 2021. Enhancing the removal efficiency of methylene blue in water by fly ash via a modified adsorbent with alkaline thermal hydrolysis treatment. RSC Adv. 11: 20292–20302.

Dogan, A.U., Dogan, M., Onal, M., Sarikaya, Y., Aburub, A. and Wurster, D.E. 2006. Baseline studies of the clay minerals society source clays: Specific surface area by the Brunauer Emmett Teller (BET) method. Clays and Clay Minerals. 54: 62–66.

Foo, K. and Hameed, B. 2010. Insights into the modeling of adsorption isotherm systems. Chem. Eng. J. 156: 2–10.

Ho, Y. and McKay, G. 1999. Pseudo-second order model for sorption processes. Process Bio. Chem. 34: 451–465.

Huang, W., Hu, Y., Li, Y., Zhou, Y., Niu, D., Lei, Z. and Zhang, Z. 2018. Citric acid-crosslinked β-cyclodextrin for simultaneous removal of bisphenol A, methylene blue and copper: The roles of cavity and surface functional groups. J. Taiwan Inst. Chem. Eng. 82: 189–197.

Islam, A.K.M.S. and Ahiduzzaman, M. 2013. Green electricity from rice husk: A model for Bangladesh. In. Tech. eBooks.

Islam, M.S., Gao, R.L., Gao, J.Y., Song, Z.T., Ali, U. and Hu, H.Q. 2022. Cadmium, lead, and zinc immobilization in soil using rice husk biochar in the presence of citric acid. Int. J. Environ. Sci. Technol. 19: 567–580.

Jackson, M.L. 1958. Soil chemical analysis. Constable and Co. Ltd.

Jiang, J., Xu, R., Jiang, T. and Li, Z. 2012. Immobilization of Cu(II), Pb(II) and Cd(II) by the addition of rice straw derived biochar to a simulated polluted Ultisol. J. Hazard. Mater. 229–230: 145–150.

Kayranli, B., Gok, O., Yilmaz, T., Gok, G., Celebi, H., Seckin, I.Y. and Mesutoglu, O.C. 2022. Low-cost organic adsorbent usage for removing Ni2+ and Pb2+ from aqueous solution and adsorption mechanisms. Int. J. Environ. Sci. Technol. 19: 3547–3564.

Kazembeigi, F., Reza, H., Arezoomand, S., Faraji, H., Mazloomi, S., Mohammadi, F., Moghadam, F., Khoshneyat, R., Nikonahad, A. and Nourmoradi, H. 2014. Removal of methylene blue from aqueous solutions using raw and modified rice husk. The Veliger. 53.

Kurniasih, M., Aprilita, N.H., Roto, R. and Mudasir, M. 2025. Modification of coal fly ash for high-capacity adsorption of methylene blue. Case Stud. Chem. Environ. Eng. 11: 101101.

Li, H., Ishak, A.R.B., Aris, M.S.B.M., Shaifuddin, S.N.B.M., Ding, S. and Deng, T. 2025. Enhanced removal of hexavalent chromium from water by nitrogen-doped wheat straw biochar

loaded with nanoscale zero-valent iron: Adsorption characteristics and mechanisms. Processes. 13: 1714.

Liang, Y., Chen, S., Zhong, J., Ding, H., Zhu, Z. and Li, S. 2022. Acid-etched coal fly ash/TiO2 nanocomposites with high photocatalytic degradation efficiency: a high value-added application of coal fly ash. J. Sol-Gel Sci. Technol. 103: 85–194.

Liu, Q., Li, Y., Chen, H., Lu, J., Yu, G., Möslang, M. and Zhou, Y. 2020. Superior adsorption capacity of functionalized straw adsorbent for dyes and heavy-metal ions. J. Hazard. Mater. 382: 121040.

Lyu, P., Li, L., Huang, X., Wang, G. and Zhu, C. 2022. Pre-magnetic bamboo biochar cross-linked Ca-Mg-Al layered double-hydroxide composite: High-efficiency removal of As(III) and Cd(II) from aqueous solutions and insight into the mechanism of simultaneous purification. Sci. Total Environ. 823: 153743.

Msimango, N.M., Makhanya, F.M., Ntola, P. and Qwabe, L.Q. 2025. Remediation of Ni(II) using sugarcane bagasse and its chemically modified derivatives: A comparison of linear and non-linear kinetic and isotherm models. Sep. Sci. Technol. 7: 899–917.

Salam, A., Shaheen, S.M., Bashir, S., Khan, I., Wang, J., Rinklebe, J., Rehman, F.U. and Hu, H. 2019. Rice straw- and rapeseed residue-derived biochars affect the geochemical fractions and phytoavailability of Cu and Pb to maize in a contaminated soil under different moisture content. J. Environ. Manage. 237: 5–14.

Zeng, W., Lu, W., Zhou, J., Zhang, J., Duan, Y., Dong, C. and Wu, W. 2024. Simultaneous removal of Cd(II) and As(V) by ferrihydrite-biochar composite: enhanced effects of As(V) on Cd(II) adsorption. J. Environ. Sci. 139: 267–280.

Zhang, H., Li, Y., Cheng, B., Ding, C. and Zhang, Y. 2020. Synthesis of a starch-based sulfonic ion exchange resin and adsorption of dyestuffs to the resin. Int. J. Biol. Macro. Mol. 161: 561–572.

Zhou, J., Li, M., Tao, Y. and Zha, L. 2025. Study on the adsorption characteristics of methylene blue by magnesium-modified fly ash. Mol. 30: 992.